remote sensing

MDPI

Communication

Multi-Frequency Interferometric Coherence Characteristics Analysis of Typical Objects for Coherent Change Detection

Zhongbin Wang [1,2], Yachao Wang [1,*], Bingnan Wang [1,2], Maosheng Xiang [1,2], Rongrong Wang [1,2], Weidi Xu [1,2] and Chong Song [1,2]

[1] National Key Laboratory of Microwave Imaging Technology, Aerospace Information Research Institute, Chinese Academy of Sciences, Beijing 100094, China; wangzhongbin17@mails.ucas.ac.cn (Z.W.); wbn@mail.ie.ac.cn (B.W.); xms@mail.ie.ac.cn (M.X.); wangrongrong18@mails.ucas.ac.cn (R.W.); xuweidi17@mails.ucas.ac.cn (W.X.); songchong18@mails.ucas.edu.cn (C.S.)

[2] School of Electronic, Electrical and Communication Engineering, University of Chinese Academy of Sciences, Beijing 100094, China

* Correspondence: wangyc@aircas.ac.cn; Tel.: +86-010-5888-7023

Abstract: This paper focuses on the study of a multi-frequency interferometric coherence characteristics analysis of typical objects for coherent change detection. Coherent change detection utilizes the phase difference between two or more SAR images to detect potential changes in the scene. It makes a difference in civilian and military applications. However, the relationship between the coherence of typical objects and SAR frequency has not been fully studied, which restricts the quality of the detection results. To address this problem, this paper conducts research on the relationship between the coherence of typical objects and SAR frequency, and the coherence characteristics are obtained through statistical analysis. In order to illustrate the relationship more clearly, the actual experimental data obtained by the DVD-InSAR system developed by the Aerospace Information Research Institute, Chinese Academy of Sciences, are utilized. The experimental results show that the coherence characteristics of typical objects are different, and this finding can provide strong support for developing change-detection applications.

Keywords: multi-frequency; synthetic aperture radar; coherence characteristics; coherent change detection

Citation: Wang, Z.; Wang, Y.; Wang, B.; Xiang, M.; Wang, R.; Xu, W.; Song, C. Multi-Frequency Interferometric Coherence Characteristics Analysis of Typical Objects for Coherent Change Detection. *Remote Sens.* **2022**, *14*, 1689. https://doi.org/10.3390/rs14071689

Academic Editor: Salvatore Stramondo

Received: 9 March 2022
Accepted: 29 March 2022
Published: 31 March 2022

1. Introduction

Synthetic aperture radar (SAR) has the characteristics of all-day, all-weather and large-area mapping [1,2], and it has been widely used in many fields. Initially, the most basic application of SAR was image formation, that is, to obtain SAR images of a certain area. With the development of SAR technology, the application of SAR has been extended to the field of target recognition [3,4], such as moving target detection [5,6], artificial target detection, and small-scale change detection [7,8]. SAR is different from other sensors in that it can acquire complex images that contain not only amplitude information but also phase information. Extracting the difference in amplitude information of SAR images between repeat-pass observations can detect large-scale changes in the scene [9], but it cannot work on any small-scale changes. However, the phase information of the SAR image is very sensitive to changes, so that it can well measure the changes in sub-wavelength level. The phase difference of the target acquired by two or more repeat-pass observations can thus be used to obtain these small-scale changes. This method adopting phase information to detect potential changes in the scene is called coherent change detection (CCD). Usually, CCD mainly utilizes the complex cross-correlation coefficient between repeat-pass interferometric synthetic aperture radar (InSAR) image pairs to detect such small amplitudes or phase changes [10–13]. It is precisely because CCD can obtain small changes in the scene that it is extremely valuable in many fields.

Among all military and civilian applications of SAR, CCD is one of the most challenging applications [14,15]. In recent years, CCD technology has been applied in numerous fields and it is followed by many researchers. The potential changes in the scene can be effectively extracted by the CCD method [16–18]. These changes may be caused by human footprints, vehicle tracks, grazing, human construction and other human activities. In addition, it may also be due to changes caused by natural disasters, such as earthquakes, flooding, landslides and other damages. Utilizing change-detection technology to extract this change information from SAR images is extremely valuable and can play an irreplaceable role in the detection of concealed targets under forest [19], human activity detection [20,21], trace detection [22], the management of illegal constructions [23], and disaster assessment [24,25].

However, due to the incomplete development of the SAR system, the relationship between the coherence of typical objects and SAR frequency has not been fully studied. As a result, the application of CCD in various fields has not yet been fully explored. The scattering mechanism of the target under SAR radiation is very complicated; different types of targets have different scattering types under the radiation of different SAR frequencies. For example, the vegetation area mainly presents the trunk part under the P-band radiation [26], while the tree canopy can be clearly observed under the Ka-band radiation. The difference in scattering mechanism will also lead to different coherence characteristics under repeat-pass observations, while there are great differences in the types of ground object contained in different regions. Therefore, it is very important to choose an appropriate frequency to observe the changed area. Choosing an appropriate frequency to observe the changed area is conducive to reliably detecting the changes of interest in the scene. On the contrary, using an inappropriate frequency for observation will result in a high false-alarm rate, a poor detection rate and unreliable detection results.

With the development of electronics technology, multi-frequency SAR systems have also appeared consecutively [27,28], which makes it possible to carry out the application and analysis concerning multi-frequency SAR systems. The Jet Propulsion Laboratory (JPL) of America and the Institute for the Electromagnetic Sensing of the Environment of the National Research Council (IREA-CNR) of Italy utilizing SIR-C/X-SAR multi-frequency system performed repeat-pass interferometric experiments in 1996 [29,30]. In 2013, the Electromagnetism and Radar Department of France also carried out relevant experiments with the RAMSES multi-frequency SAR system. Lately, the German Aerospace Center conducted the ARCTIC 2015 campaign and the AfriSAR 2016 campaign with an advanced airborne F-SAR system [31–33]. In addition, other researchers have also studied interferometric applications with a multi-frequency satellite SAR system [34–36], such as Sentinel-1, Radarsat-2 and TerraSAR-X. The difference is that these acquisitions are not contemporaneous, which introduces the extra dimension of temporal variability into the data [37].

The relationship between the coherence of typical objects and SAR frequency is very valuable and significant for the change-detection application. However, the relationship has not been fully studied until now. This paper focuses on the relationship between the coherence of typical objects and SAR frequency. A large number of experiments have been carried out and effective experimental data have been obtained with the DVD-InSAR system which can observe the same scene at six frequencies simultaneously. Combining all six or more frequencies into one airborne SAR system had not been done before. This study will make it possible for researchers to compare the radar backscatter characteristics and study coherence characteristics across frequencies simultaneously. The relationship between the coherence of different typical objects and SAR frequency is analyzed in detail in this paper.

In this paper, we present an analysis of multi-frequency interferometric coherence characteristics of typical objects for coherent change detection. In Section 2 of this paper, we discuss the method for multi-frequency interferometric processing. Section 3 presents the experimental results and analysis of the work. In Section 4, this paper is concluded and a discussion of this work is provided.

2. Methodology

This paper focuses on the analysis of multi-frequency interferometric coherence characteristics of typical objects. The whole process is shown in Figure 1. The processing mainly includes three steps. Firstly, using SAR raw data, an external digital elevation map (DEM) and orbital parameters are used to obtain focused SAR image pairs. Then, the image registration, interferometric processing and coherence estimation are performed for the focused SAR image pairs to obtain the coherence map. Finally, the coherence characteristics of typical objects are analyzed through statistical analysis and the coherence characteristics curve of typical objects is presented eventually.

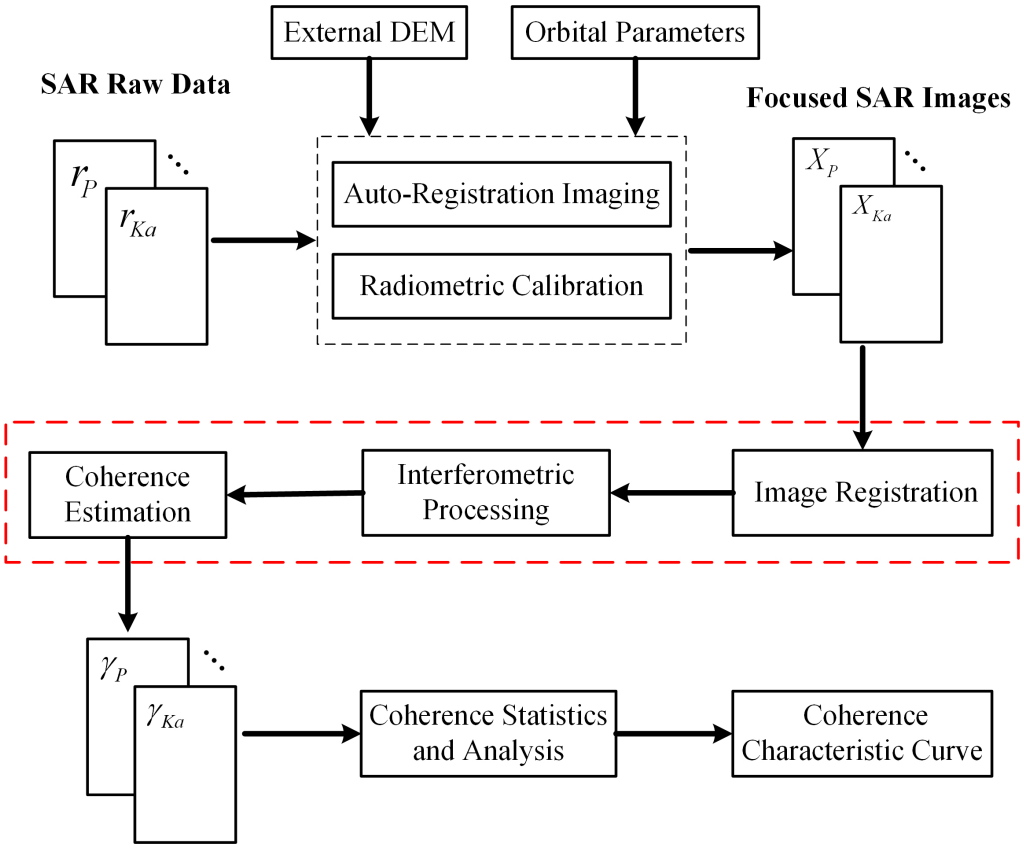

Figure 1. The whole process of the multi-frequency interferometric coherence characteristics analysis of typical objects for coherent change detection.

2.1. Auto-Registration Imaging

The systematic parameters of the multi-frequency SAR system are different, which can cause different ranges and azimuth pixel spacing of SAR images at each frequency. The same target will have a certain position offset under the observation of SAR systems of different frequencies because of the different sampling delay errors and the different antenna phase center. In order to analyze the relationship between the interferometric coherence of typical objects and SAR frequency, it is necessary to obtain the registered multi-frequency SAR images of the study area with the same pixel spacing. At the same time, it is necessary to maintain the accuracy of the imaging results in terms of focus, radiation, phase, etc. Utilizing the unique characteristics of observational geometry and consistent timing of the multi-frequency SAR system is an effective way to achieve auto-registration imaging.

Primarily, the inconsistent sampling time delay errors of the radar systems with various frequencies result in different errors in the slant range. In order to obtain a consistent slant range, the sampling time delay of different SAR systems has to be calibrated according

to the internal calibration signal recorded by the raw data. This ensures that the SAR images acquired at different SAR subsystems have the same slant range for a given target.

Since the multi-frequency SAR system has consistent timing characteristics, it is beneficial to obtain multi-frequency SAR images with excellent phase consistencies and high degrees of overlap. However, the pulse repetition frequency (PRF) of SAR systems of different frequencies is always different, resulting in different pixel spacing in the azimuth direction of multi-frequency SAR images. In order to obtain the same pixel spacing in the azimuth direction, the same PRF should be chosen for imaging. In addition, the antenna phase centers of different SAR systems are inconsistent, which means that the installation positions of the antennas are separated. In order to make the pixel offset of the multi-frequency SAR images in the azimuth direction as small as possible, the same period of time was selected as the imaging time interval for each of the SAR subsystems, which can simplify the complexity of image registration among SAR images of different frequencies. The pixel position offset along the azimuth direction was obtained according to the different initial mounting positions of the antennas, so that the multi-frequency SAR images could realize auto-registration imaging in the azimuth direction.

Because the bandwidth and sampling rate of each subsystem are different, the pixel spacing and resolution in the range direction of multi-frequency SAR images are not identical. In order to make SAR images have the same pixel spacing in the range direction, the same sampling rate should be chosen for imaging. At the same time, due to the inconsistent phase centers of the antennas of different SAR systems, the pixel position of the multi-frequency SAR images along the range direction was deviated. The offset along the range direction was calculated according to the initial installation position of the antenna of different SAR systems, so that the multi-frequency SAR images could realize the auto-registration in the range direction.

To date, the multiple SAR images acquired in multi-frequency SAR systems have the same pixel position. This allows the researchers conveniently to compare and analyze the scattering characteristics of the interesting target. The aim is for a specific SAR application in which the appropriate frequency is chosen to perform the scientific missions in the future.

Temporal decorrelation is an important representation of the stability of the target. Under the above processing, the multi-frequency SAR datasets obtained from repeat-pass observations are imaged in turn. Then, the multi-frequency master and slave SAR images of the study area are obtained in turn.

2.2. Interferometric Processing and Analysis

Due to the different installation positions of the antenna of the SAR subsystem on the aircraft, there is a slight time difference when the SAR subsystem of each band observes the same region on the ground. Using the same period of time for coincident imaging causes several pixels to become offset among SAR images of different frequencies in the azimuth direction. In order to align the pixel position among SAR images of different frequencies as much as possible, it is necessary to achieve at least pixel-level registration for multi-frequency SAR images. Generally, the geometric relationship among the antenna of the multi-frequency SAR systems is applied to register the multi-frequency SAR images.

The interferometric processing mainly includes repeat-pass InSAR image registration and coherence estimation. The repeat-pass InSAR image registration is to achieve a high precision of alignment, and the registration accuracy should be at least 1/8 pixel [38]. If there are some registration errors, even sub-pixel-level mismatch will lead to a decrease in coherence and phase noise, which will seriously affect the quality of the interferogram. In this paper, the maximum complex coherence coefficient method is adopted to realize the registration between the repeat-pass InSAR image pairs for each frequency in turn. The coherence estimation is to obtain a measure of the degree of coherence between repeat-pass InSAR image pairs.

Assuming that the two SAR images obtained by repeat-pass InSAR observations are X_{1k} and X_{2k}, after the repeat-pass InSAR image registration, the coherence between the two images is defined as the magnitude of the normalized complex cross-correlation coefficient. This is given as [39,40]:

$$\gamma = \left| \frac{E\left[X_{1k}^{H} X_{2k}\right]}{\sqrt{E\left[{X_{1k}}^{2}\right] E\left[{X_{2k}}^{2}\right]}} \right| \tag{1}$$

where $E[\cdot]$ is the expectation operator and A^H denotes the conjugate of a variable A. In practice, the expectation in Equation (1) is generally substituted by the mean sample operator, and a window around the pixel neighborhood is used [41,42].

$$\gamma = \left[\frac{\Sigma_N X_{1k}^{H} X_{2k}}{\sqrt{\Sigma_N {X_{1k}}^{2} \Sigma_N {X_{2k}}^{2}}} \right] \tag{2}$$

The scattering characteristics of typical objects are not only related to their own material and surface structure, but also the frequency and polarization of electromagnetic waves. The scattering characteristics of typical objects dominated by surface scattering are mainly related to surface roughness, soil dielectric constant and SAR frequency. The typical objects mainly scattered by volume scattering are closely associated with the scattering type and penetration depth of the electromagnetic wave.

In order to understand the interaction process and mechanism between electromagnetic waves and typical objects more clearly, especially the coherence characteristics between typical objects and different SAR frequencies, sufficient samples of each typical object were selected in the study area. The average coherence of each type of typical object was calculated according to the coherence coefficient map obtained from the interferometric processing. Then, the relationship between the coherence characteristics of each typical object and SAR frequency was presented through statistical analysis.

3. Experiments and Results

To analyze the coherence characteristics of typical objects on the ground, one set of six-band airborne InSAR data is used in this paper. The experimental results and analysis are presented in this section. In addition, in order to illustrate the coherence characteristics more sufficiently, the dataset acquired in vegetation regions is analyzed as well.

3.1. Experiments

The coherence of different typical objects has different trends with the variation of SAR frequency. In order to present these trends and make clearer and more intuitive judgments, this section introduces the selected study area and experimental dataset in detail for further analysis.

This paper selected an area with many typical objects as the study area. This area is located in Gansu Province, China. The Google map and SAR amplitude image of the study area are shown in Figure 2. This area contains general types of typical objects, such as vegetation, buildings, bare land and other types. At the same time, this area is located at the junction of city and desert. Studying the coherence of this area is not only significant for change detection in the urban environment, but also of great significance for change detection in the desert and underpopulated land environment. In addition, the soil in the study area is relatively dry, which can ensure that the acquired SAR images have relatively good coherence.

(**a**) (**b**)

Figure 2. (**a**) Google map and (**b**) SAR amplitude image of the study area.

Most land cover types on the ground show obvious scattering differences under the irradiation of electromagnetic waves at different frequencies. The amplitude of the electromagnetic return depends on the electromagnetic structure of the target, while the coherence is mostly related to its mechanical stability. The interferometric coherence is more valuable for the study of scattering targets, and it can provide better discrimination for SAR applications. In order to study the relationship between the coherence of typical objects and SAR frequency, the DVD-InSAR system developed by the Aerospace Information Research Institute, Chinese Academy of Sciences, was used to carry out experiments in Gansu Province, China, in October 2020. A large amount of experimental data was obtained for different scientific missions, especially where the multi-frequency repeat-pass InSAR data were obtained to study the frequency characteristics of interferometric coherence and other applications, such as the classification, tomography and target recognition. The DVD-InSAR system is composed of six SAR subsystems at P, L, S, C, X and Ka bands, where the system works with the same frequency source to ensure the consistency of timing and phase between different subsystems. Meanwhile, the geometric position on board the antennas is well measured. The DVD-InSAR system is mounted on the Modern Ark 60 (MA60) aircraft platform. An optical image of the platform is shown in Figure 3.

Figure 3. The aircraft platform of the DVD-InSAR system.

The DVD-InSAR system has multiple working modes, including strip-map, spotlight, cross-track and along-track interferometry modes. The six-band SAR subsystems share a set of positioning and orientation systems (POS) and have the same timing source. These six-band SAR systems can work at the same time and acquire SAR images of the same scene simultaneously. Table 1 shows the main parameters of the DVD-InSAR system. The carrier frequency, bandwidth and pulse repetition frequency are different for each SAR subsystem, which results in different resolutions. In addition, the pixel spacing is set to identical, which is 0.393 m and 0.468 m in the azimuth and range directions, respectively.

Table 1. Main parameters of DVD-InSAR system.

Parameter	Value
SAR band	P \ L \ S \ C \ X \ Ka
Carrier frequency	0.39\0.96\3.2\5.4\9.6\35 GHz
Bandwidth	200\200\300\300\500\600 MHz
Pulse repetition frequency	500\2000\1000\500\1000\2000 Hz
Resolution	1\1\1\0.5\0.5\0.3 m
Look angle	45°
Platform velocity	98.15 m/s
Azimuth pixel spacing	0.393 m
Range pixel spacing	0.468 m

The temporal decorrelation of the targets characterizes their mechanical and dielectric stability. It is very critical to study the temporal decorrelation to better develop scientific missions in the future. In order to analyze the relationship between the temporal decorrelation and SAR frequency of the selected study area in this paper, we chose the repeat-pass interferometry observation mode of the DVD-InSAR system to obtain an experimental dataset. Multiple flights were conducted in the selected study area with the DVD-InSAR system.

The SAR backscatter intensity of the ground target is a function of several factors, including the SAR wavelength, image acquisition geometry, local topography, surface roughness and the dielectric constant of the targets [43,44]. In order to show the relationship between the coherence characteristics of typical objects and SAR frequency more clearly and directly, this paper selected a typical area containing multiple land cover types as the study area, mainly including building, road, railway, vegetation, bare land and water regions.

Firstly, the multi-frequency datasets obtained by the DVD-InSAR system were used to obtain the auto-registered SAR images of the selected study area, and the six-band SAR images with the same pixel spacing were obtained. Due to a certain offset of the installation position among antennas of multi-frequency SAR systems, there was always a certain pixel offset of the study area in the azimuth direction. Considering the installation position of the P-band antenna as a reference, the pixel position offset of SAR images of other bands relative to the P-band SAR image was calculated according to the installation positions between other antennas and the P-band antenna. This means that the pixel position offset could be calculated between the installation positions of multiple antennas. Then, the six-band SAR images were registered in the azimuth direction. Then, through choosing the same sampling rate and upsampling or desampling the SAR images, identical pixel spacing in the range direction was ensured. The pixel offset in the range direction could also be corrected according to the installation position of the antennas.

Secondly, due to the two-dimensional distortion between the two SAR images obtained by the repeat-pass observations, the maximum coherence coefficient method was used to realize the interferometric image registration between the master and slave images. With Equation (2), the coherence of the repeat-pass image pairs after registration was estimated for each SAR band in turn. The coherence coefficient maps of each SAR band are shown in Figure 4.

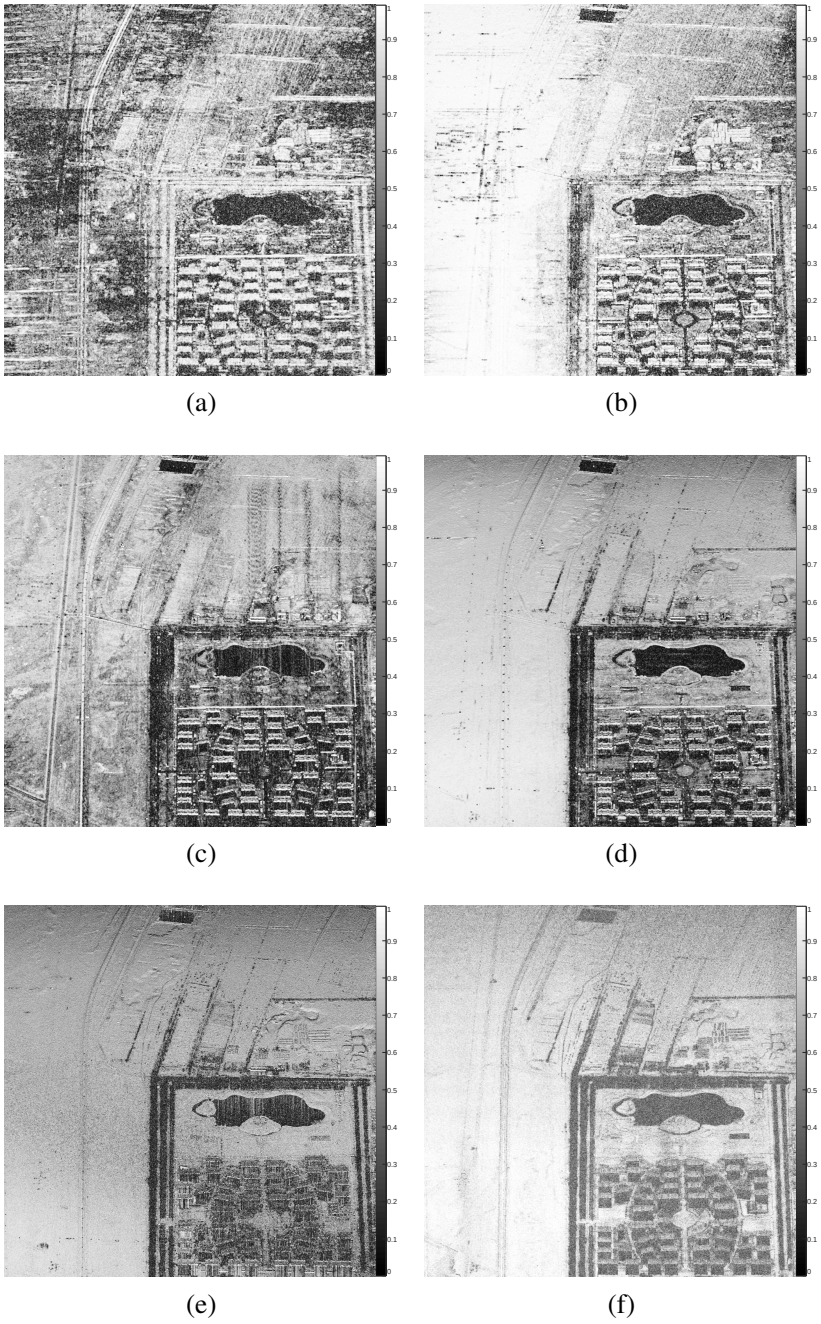

Figure 4. Coherence maps of the study area. (**a**) P-band. (**b**) L-band. (**c**) S-band. (**d**) C-band. (**e**) X-band. (**f**) Ka-band.

As shown in Figure 4, the coherence of different typical objects has different values at different SAR frequencies, which means that the coherence characteristics of each typical object are different varying with SAR frequencies. There are many SAR applications which are closely related to the interferometric coherence. For example, the interferometric coherence is regarded as a vital measurement to locate, extract and recognize the changed areas for coherent change-detection applications. However, the interesting types of detected typical object are always different, so that studying and analyzing the coherence characteristics will help us better detect the areas.

3.2. Experiment Analysis

In order to fully analyze the coherence characteristics, sufficient samples of different typical objects were first selected from the coherence map of the study area. The typical

objects mainly included building, vegetation, bare land, road, railway and water regions. Table 2 shows the samples of the different typical objects. Then, the average coherence of different typical objects was calculated through the selected samples. The statistical results are shown in Figure 5. It can be seen that the coherence of different typical objects has different frequency characteristics.

Table 2. The samples of different typical objects.

	Building	Vegetation	Bare Land	Road	Railway	Water
Pixels	4360	399,500	29,850	11,480	1370	1300

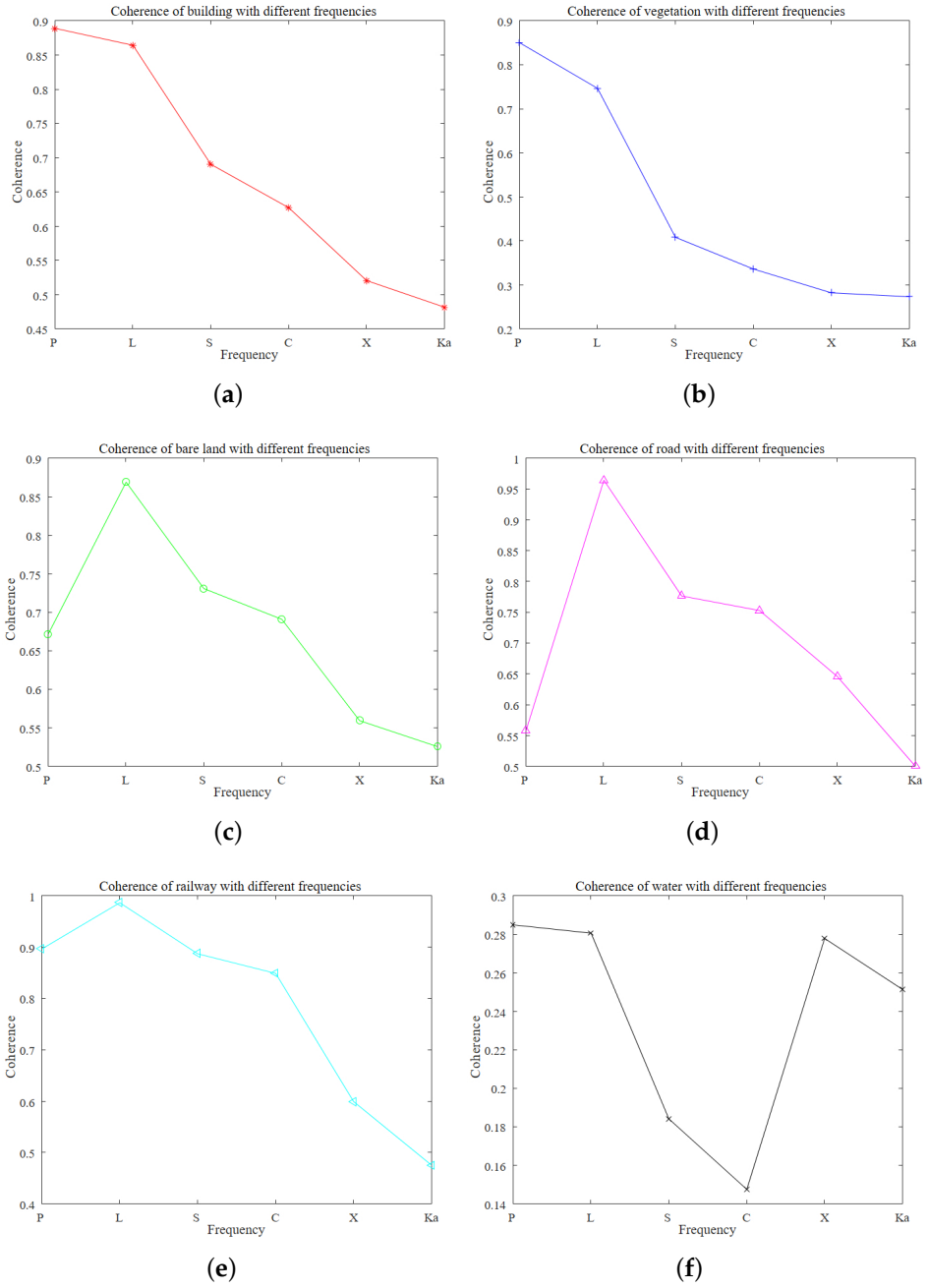

Figure 5. Coherence statistics of typical objects. (**a**) Building region. (**b**) Vegetation region. (**c**) Bare land region. (**d**) Road region. (**e**) Railway region. (**f**) Water region.

As shown in Figure 5, the interferometric coherence was influenced to a greater degree by the SAR frequency in all types of typical objects, where the temporal baseline of the InSAR images was the same, at about two hours. The influence of the spatial baseline was compensated in the total coherence. Therefore, the interferometric coherence can express the state change of typical objects. Analyzing the coherence characteristics would offer significant guidance for future SAR applications.

For the building and vegetation regions, the coherence decreased with the increase in SAR frequency. The building regions had a high coherence in all frequencies, as expected, whereas the coherence characteristics of the building regions were closely related to the roughness in various electromagnetic waves. Generally, the roughness of the buildings was higher at low frequencies, so that the coherence was higher at low frequencies than at high frequencies. The coherence characteristics of the vegetation regions were mainly related to the scattering type and penetration depth in various electromagnetic waves, whereas high frequencies, such as the Ka-band and X-band, did not penetrate into the forest volume, and the scattering energy from the branches and leaves on the top of the trees was dominant. The movement of the tree leaves between the two acquisitions produced a degradation in the coherence. Conversely, low frequencies, such as the P-band and L-band, could penetrate into the forest volume, and the scattering type was mainly double-bounce and surface scattering.

For the bare land, road and railway regions, the coherence characteristics followed a similar trend with variations in SAR frequency. This was because the scattering type of these regions was mainly surface scattering. Due to the stronger penetration ability of P-band electromagnetic waves in these regions, the scattering energy was severely degraded, which resulted in the coherence of the P-band being lower than that of the L-band, as shown in Figure 5. In general, the lower the frequency and the lower the soil moisture, the greater the penetration depth. Even though the trend was similar in these three regions, the coherence level was distinct in different regions. This was because the roughness, scattering characteristics and soil moisture were not completely consistent. Especially, the stability and the penetration ability of the P-band in these three regions were not the same, which resulted in a great difference in the coherence.

For the water region, the coherence was seriously lower than other types of typical objects shown in Figure 5. The reason is that the specular scattering was dominant in the calm water region, which resulted in the scattering energy being generally weak. In fact, the echo received by the SAR system and reflected by the water region was similar to noise, where the phase was not reliable and was random. Therefore, the stability in the water region was poor, so that the coherence of the region presented random characteristics.

CCD utilizes coherence to extract the changed area in the study area. The study of the relationship between the coherence of typical objects and SAR frequency is beneficial to the further development of change-detection applications. Since the area of interest usually contains different types of major objects, a clear study of this relationship can effectively guide us in choosing the appropriate one or several SAR frequencies to observe the changed area of interest. False alarms and correct detection are the main attention in the CCD application. If a fine detection result is expected, the false alarms should be reduced from the final detection results.The detection results are always seriously corrupted by false alarms, which can be avoided through choosing the appropriate frequency according to the changed object types. For example, if the changed areas are dominated by buildings and vegetation types, the P-band or L-band should be preferred; if the changed areas are dominated by the bare land type, the L-band, C-band or X-band should be preferred. In short, choosing the appropriate SAR frequency helps in obtaining more reliable detection results.

In order to further illustrate the difference in frequency characteristics in CCD, the SAR dataset acquired in the vegetation regions was utilized to compare the performance difference. The dataset was acquired by the P-band and C-band SAR system in vegetation regions, where the change was mainly the movement of vehicles. The main land cover type

was vegetation and bare land, which were not the types of interest. These two types were expected in high coherence to obtain the actual change of vehicles. If inappropriate frequencies are used for observation, there will be more false alarms in the detection results. The mission and reference SAR images of the vegetation regions are shown in Figures 6 and 7.

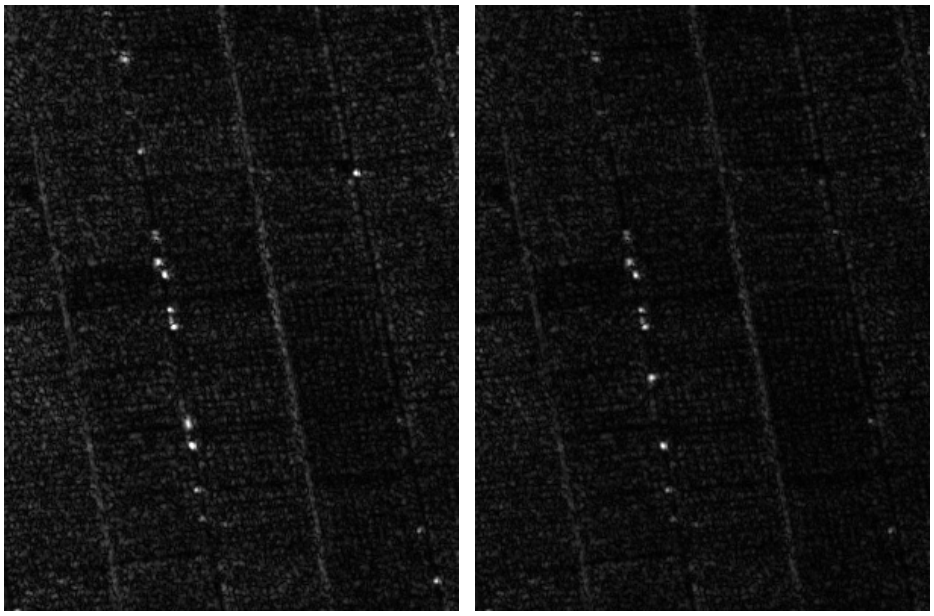

(**a**) (**b**)

Figure 6. The P-band SAR images of the experimental scene. (**a**) Reference SAR image. (**b**) Mission SAR image.

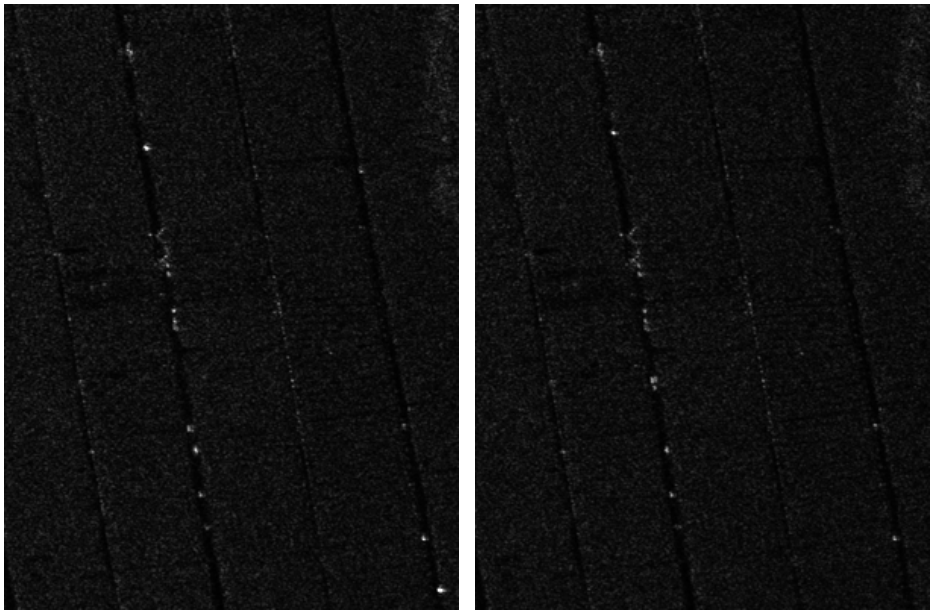

(**a**) (**b**)

Figure 7. The C-band SAR images of the experimental scene. (**a**) Reference SAR image. (**b**) Mission SAR image.

By performing interferometric processing and coherence estimation on the P-band and C-band SAR image pairs, respectively, the coherence map was obtained as shown in Figure 8. It can be seen from Figure 8 that the coherence of the vegetation region showed a significant difference between the P-band and the C-band, which was due to the great

difference in the mechanical stability of the target across different frequencies. As is shown in Figure 5b, the coherence of the vegetation region was higher in the P-band than in the C-band, which resulted in fewer false alarms.

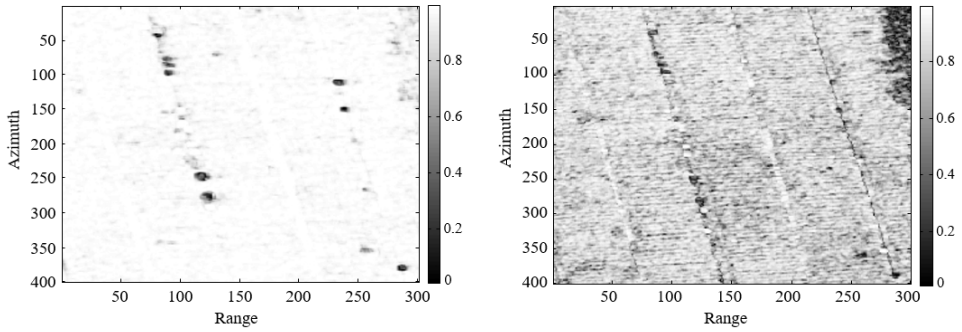

(**a**) (**b**)

Figure 8. Coherence map of the vegetation region. (**a**) P-band and (**b**) C-band.

Then, in order to show the difference between the P-band and the C-band on CCD more sufficiently, a detection result was obtained by thresholding the coherence map. The detection results for the P-band and the C-band are shown in Figure 9. The black area in Figure 9a is mainly the movement of vehicles, including arrival and departure, while the black area in Figure 9b includes the movement of the vehicle and false alarms caused by vegetation in the scene.

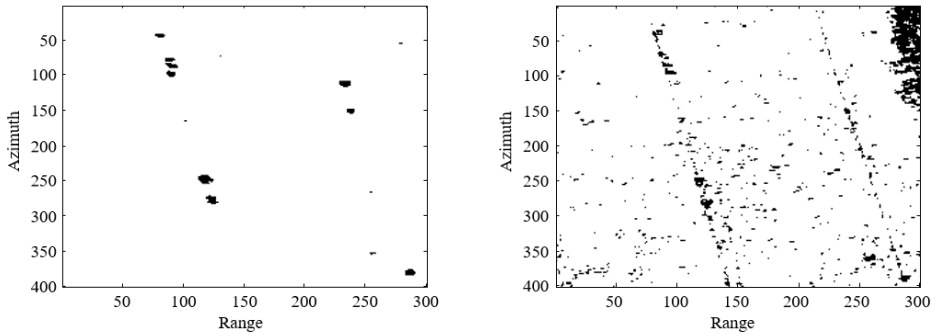

(**a**) (**b**)

Figure 9. Results comparison between P-band and C-band. (**a**) P-band and (**b**) C-band.

Finally, in order to clearly show the performance difference between the P-band and the C-band, the detection results in Figure 9 are compared with the ground truth overlay in Figure 10. It can be concluded that the C-band had more false alarms than the P-band, mainly due to the swing of tree leaves in the scene. The experimental results show that the P-band results can detect the potential movements of vehicles more effectively in comparison with the C-band; the C-band results had more false alarms. Therefore, if our goal is to study the CCD in vegetated regions, the P-band is preferred, since it leads to less decorrelation in vegetated regions.

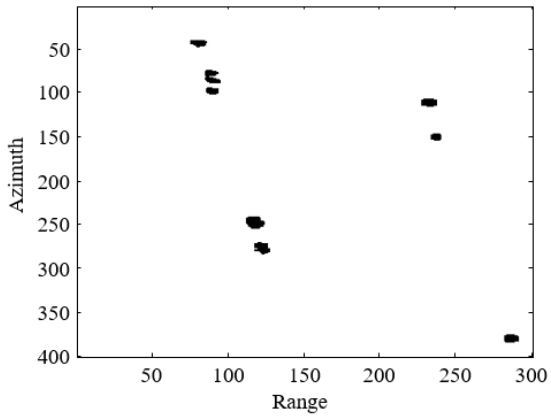

Figure 10. The ground truth overlay.

4. Discussion

CCD technology has been widely used in civilian and military fields. Acquiring change information makes a great difference in many applications, such as subtle human activity detection, illegal construction management and disaster assessment. However, the coherence characteristics of typical objects has not yet been fully studied, which restricts the quality of the detection results.

In order to solve this problem, we conducted a study on multi-frequency interferometric coherence characteristics analysis of typical objects. The coherence characteristics were obtained through statistical analysis, while the data were acquired through the DVD-InSAR system developed by the Aerospace Information Institute, Chinese Academy of Sciences, and were utilized to show the coherence characteristics more clearly. We selected building, vegetation, bare land, road, railway and water regions as the typical objects for the analysis.

The experimental results show that the coherence characteristics of typical objects are different. For building and vegetation regions, the coherence decreased with increases in SAR frequency. For bare land, road and railway regions, the coherence characteristics followed a similar trend with variations in SAR frequency. For the water region, the coherence characteristics were irregular.

Particularly, in order to illustrate the difference in the frequency characteristics in the application of CCD, the dataset acquired in the vegetation region was utilized to compare the difference. The results showed that there were more false alarms in the C-band than in the P-band. Therefore, if our goal is to study the CCD in vegetation regions, P-band SAR is to be preferred.

In this paper, we only analyzed the differences in the coherence characteristics among different SAR frequencies. This will allow scientists to select one or several SAR frequencies for observation according to the given set of science drivers for future missions. However, the connection and complementation of the coherence characteristics also deserve study. In future research, we will consider the situation to further improve the CCD results. In order to better develop scientific missions, multi-frequency interferometric coherence characteristics deserve more careful study in the future.

Author Contributions: All the authors made contributions to the article in different areas. Conceptualization, B.W., M.X. and Y.W.; investigation, Z.W.; software, Z.W. and C.S.; writing—original draft preparation, Z.W.; writing—review and editing, Z.W., W.X. and R.W. All authors have read and agreed to the published version of the manuscript.

Funding: This work was supported by the National Natural Science Foundation of China under Grant No. 62073306 and Grant No. 61991424. This work was also supported by the Youth Innovation Promotion Association CAS.

Institutional Review Board Statement: Not applicable.

Informed Consent Statement: Not applicable.

Data Availability Statement: Data sharing not applicable.

Acknowledgments: The authors would like to thank the staff of the National Key Laboratory of Microwave Imaging Technology, Aerospace Information Research Institute, Chinese Academy of Sciences, for their valuable conversations and comments.

Conflicts of Interest: The authors declare no conflict of interest.

References

1. Moreira, A.; Prats-Iraola, P.; Younis, M.; Krieger, G.; Hajnsek, I.; Papathanassiou, K.P. A tutorial on synthetic aperture radar. *IEEE Geosci. Remote Sens. Mag.* **2013**, *1*, 6–43. [CrossRef]
2. Hu, Z.; Bryant, M.; Qiu, R.C. Multi-path SAR change detection. In Proceedings of the 2012 IEEE Radar Conference, Atlanta, GA, USA, 7–11 May 2012; pp. 859–863. [CrossRef]
3. Dong, G.; Kuang, G.; Wang, N.; Zhao, L.; Lu, J. SAR Target Recognition via Joint Sparse Representation of Monogenic Signal. *IEEE J. Sel. Top. Appl. Earth Obs. Remote Sens.* **2015**, *8*, 3316–3328. [CrossRef]
4. Yu, M.; Dong, G.; Fan, H.; Kuang, G. SAR Target Recognition via Local Sparse Representation of Multi-Manifold Regularized Low-Rank Approximation. *Remote Sens.* **2018**, *10*, 211. [CrossRef]
5. Yang, J.; Liu, C.; Wang, Y. Detection and Imaging of Ground Moving Targets With Real SAR Data. *IEEE Trans. Geosci. Remote Sens.* **2015**, *53*, 920–932. [CrossRef]
6. Li, Z.; Wu, J.; Liu, Z.; Huang, Y.; Yang, H.; Yang, J. An Optimal 2-D Spectrum Matching Method for SAR Ground Moving Target Imaging. *IEEE Trans. Geosci. Remote Sens.* **2018**, *56*, 5961–5974. [CrossRef]
7. Wahl, D.E.; Yocky, D.A.; Jakowatz, C.V.; Simonson, K.M. A New Maximum-Likelihood Change Estimator for Two-Pass SAR Coherent Change Detection. *IEEE Trans. Geosci. Remote Sens.* **2016**, *54*, 2460–2469. [CrossRef]
8. Tzouvaras, M.; Danezis, C.; Hadjimitsis, D.G. Small Scale Landslide Detection Using Sentinel-1 Interferometric SAR Coherence. *Remote Sens.* **2020**, *12*, 1560. [CrossRef]
9. Mian, A.; Collas, A.; Breloy, A.; Ginolhac, G.; Ovarlez, J.P. Robust Low-Rank Change Detection for Multivariate SAR Image Time Series. *IEEE J. Sel. Top. Appl. Earth Obs. Remote Sens.* **2020**, *13*, 3545–3556. [CrossRef]
10. Yu, B.; Phillips, R.D. Using contextual information to improve SAR CCD: Bayesian contextual coherent change detection (BC CCD). In Proceedings of the 2014 IEEE Geoscience and Remote Sensing Symposium, Quebec City, QC, Canada, 13–18 July 2014; pp. 1277–1280. [CrossRef]
11. Newey, M.; Barber, J.; Benitz, G.; Kogon, S. False alarm mitigation techniques for SAR CCD. In Proceedings of the 2013 IEEE Radar Conference, Ottawa, ON, Canada 29 April–3 May 2013; pp. 1–6. [CrossRef]
12. Horst, H.; Lorenz, F.; Cadario, E.; Kuny, S.; Thiele, A. Enhancement of Coherence Images for Coherent Change Detection. In Proceedings of the EUSAR 2021, 13th European Conference on Synthetic Aperture Radar, Leipzig, Germany, 29 March–1 April 2021; pp. 1–6.
13. Biondi, F. (L + S)-RT-CCD for Terrain Paths Monitoring. *IEEE Geosci. Remote Sens. Lett.* **2018**, *15*, 1209–1213. [CrossRef]
14. Carotenuto, V.; Clemente, C.; De Maio, A.; Soraghan, J.; Iommelli, S. Multi-polarization SAR change detection: Unstructured versus structured GLRT. In Proceedings of the 2014 Sensor Signal Processing for Defence, Edinburgh, UK, 8–9 September 2014; pp. 1–5. [CrossRef]
15. Biondi, F. A new maximum likelihood polarimetric interferometric synthetic aperture radar coherence change detection (ML-PolInSAR-CCD). *Int. J. Remote Sens.* **2019**, *40*, 5158–5178. [CrossRef]
16. Cha, M.; Phillips, R.; Wolfe, P.J. Test statistics for synthetic aperture radar coherent change detection. In Proceedings of the 2012 IEEE Statistical Signal Processing Workshop, Ann Arbor, MI, USA, 5–8 August 2012; pp. 856–859. [CrossRef]
17. Monti-Guarnieri, A.V.; Brovelli, M.A.; Manzoni, M.; d'Alessandro, M.M.; Molinari, M.E.; Oxoli, D. Coherent Change Detection for Multipass SAR. *IEEE Trans. Geosci. Remote Sens.* **2018**, *56*, 6811–6822. [CrossRef]
18. Manzoni, M.; Monti-Guarnieri, A.; Molinari, M.E. Joint exploitation of spaceborne SAR images and GIS techniques for urban coherent change detection. *Remote Sens. Environ.* **2021**, *253*, 112152. [CrossRef]
19. Pincus, P.B.; Preiss, M. Coherent change detection under a forest canopy. In Proceedings of the 2018 International Conference on Radar, Brisbane, QLD, Australia 27–31 August 2018; pp. 1–6. [CrossRef]
20. Wang, Z.; Wang, Y.; Wang, B.; Hu, X.; Song, C.; Xiang, M. Human Activity Detection Based on Multipass Airborne InSAR Coherence Matrix. *IEEE Geosci. Remote Sens. Lett.* **2022**, *19*, 1–5. [CrossRef]
21. Hammer, H.; Kuny, S.; Thiele, A. Enhancing Coherence Images for Coherent Change Detection: An Example on Vehicle Tracks in Airborne SAR Images. *Remote Sens.* **2021**, *13*, 5010. [CrossRef]
22. Zhang, J.; Xing, M.; Sun, G.C.; Wang, Z. Multiple Statistics Contributing to Few-Sample Deep Learning for Subtle Trace Detection in High-Resolution SAR Images. *IEEE Trans. Geosci. Remote Sens.* **2022**, *60*, 1–14. [CrossRef]
23. Zhang, K.; Fu, X.; Lv, X.; Yuan, J. Unsupervised Multitemporal Building Change Detection Framework Based on Cosegmentation Using Time-Series SAR. *Remote Sens.* **2021**, *13*, 471. [CrossRef]

24. Oxoli, D.; Boccardo, P.; Brovelli, M.A.; Molinari, M.E.; Monti Guarnieri, A. Coherent change detection for repeated-pass interferometric SAR images: An application to earthquake damage assessment on buildings. *Int. Arch. Photogramm. Remote Sens. Spat. Inf. Sci.* **2018**, *502*, 383–388. [CrossRef]
25. Washaya, P.; Balz, T.; Mohamadi, B. Coherence Change-Detection with Sentinel-1 for Natural and Anthropogenic Disaster Monitoring in Urban Areas. *Remote Sens.* **2018**, *10*, 1026. [CrossRef]
26. Liu, C.; Yin, J.; Yang, J.; Gao, W. Classification of multi-frequency polarimetric SAR images based on multi-linear subspace learning of tensor objects. *Remote Sens.* **2015**, *7*, 9253–9268. [CrossRef]
27. Wu, Y. Concept on Multidimensional Space Joint-observation SAR. *J. Radars* **2013**, *2*, 135–142. [CrossRef]
28. Ding, C.; Qiu, X.; Wu, Y. Concept, system, and method of holographic synthetic aperture radar. *J. Radars* **2020**, *3*, 399–408. [CrossRef]
29. Rosen, P.A.; Hensley, S.; Zebker, H.A.; Webb, F.H.; Fielding, E.J. Surface deformation and coherence measurements of Kilauea Volcano, Hawaii, from SIR-C radar interferometry. *J. Geophys. Res. Planets* **1996**, *101*, 23109–23125. [CrossRef]
30. Lanari, R.; Fornaro, G.; Riccio, D.; Migliaccio, M.; Papathanassiou, K.; Moreira, J.; Schwabisch, M.; Dutra, L.; Puglisi, G.; Franceschetti, G.; et al. Generation of digital elevation models by using SIR-C/X-SAR multifrequency two-pass interferometry: the Etna case study. *IEEE Trans. Geosci. Remote Sens.* **1996**, *34*, 1097–1114. [CrossRef]
31. Reigber, A.; Jäger, M.; Krogager, E. Polarimetric SAR change detection in multiple frequency bands for environmental monitoring in Arctic regions. In Proceedings of the 2016 IEEE International Geoscience and Remote Sensing Symposium (IGARSS), Beijing, China, 10–15 July 2016; pp. 5702–5705. [CrossRef]
32. Horn, R.; Jaeger, M.; Keller, M.; Limbach, M.; Nottensteiner, A.; Pardini, M.; Reigber, A.; Scheiber, R. F-SAR—Recent upgrades and campaign activities. In Proceedings of the 2017 18th International Radar Symposium (IRS), Prague, Czech Republic, 28–30 June 2017; pp. 1–10. [CrossRef]
33. Henke, D.; Dominguez, E.M.; Fagir, J.; Fritsche, L.; Horn, R.; Scheiber, R.; Reigber, A.; Sieger, S.; Janssen, D.; Klöppel, F.; et al. Multi-Platform, Multi-Frequency SAR Campaign with the F-SAR and Miranda35 Sensors. In Proceedings of the IGARSS 2020 IEEE International Geoscience and Remote Sensing Symposium, Waikoloa, HI, USA, 26 September–2 October 2020; pp. 6166–6169. [CrossRef]
34. Martinis, S.; Fissmer, B.; Rieke, C. Time series analysis of multi-frequency SAR backscatter and bistatic coherence in the context of flood mapping. In Proceedings of the 2015 8th International Workshop on the Analysis of Multitemporal Remote Sensing Images (Multi-Temp), Annecy, France, 22–24 July 2015; pp. 1–4. [CrossRef]
35. Maleki, S.; Baghdadi, N.; Soffianian, A.; El Hajj, M.; Rahdari, V. Analysis of multi-frequency and multi-polarization SAR data for wetland mapping in Hamoun-e-Hirmand wetland. *Int. J. Remote Sens.* **2020**, *41*, 2277–2302. [CrossRef]
36. Hagensieker, R.; Waske, B. Evaluation of Multi-Frequency SAR Images for Tropical Land Cover Mapping. *Remote Sens.* **2018**, *10*, 257. [CrossRef]
37. Freeman, A.; Zink, M.; Caro, E.; Moreira, A.; Veilleux, L.; Werner, M. The legacy of the SIR-C/X-SAR radar system: 25 years on. *Remote Sens. Environ.* **2019**, *231*, 111255. [CrossRef]
38. Fang, D.; Lv, X.; Yun, Y.; Li, F. An InSAR Fine Registration Algorithm Using Uniform Tie Points Based on Voronoi Diagram. *IEEE Geosci. Remote Sens. Lett.* **2017**, *14*, 1403–1407. [CrossRef]
39. Wei, M.; Sandwell, D.T. Decorrelation of L-Band and C-Band Interferometry Over Vegetated Areas in California. *IEEE Trans. Geosci. Remote Sens.* **2010**, *48*, 2942–2952. [CrossRef]
40. Sabry, R. Improving SAR-Based Coherent Change Detection Products by Using an Alternate Coherency Formalism. *IEEE Geosci. Remote Sens. Lett.* **2021**, *18*, 1054–1058. [CrossRef]
41. Touzi, R.; Lopes, A.; Bruniquel, J.; Vachon, P.W. Coherence estimation for SAR imagery. *Geosci. Remote Sens. IEEE Trans.* **1999**, *37*, 135–149. [CrossRef]
42. Lê, T.T.; Froger, J.; Hrysiewicz, A.; Paris, R. Coherence Change Analysis for Multipass Insar Images Based on the Change Detection Matrix. In Proceedings of the IGARSS 2019 IEEE International Geoscience and Remote Sensing Symposium, Yokohama, Japan, 28 July–2 August 2019; pp. 1518–1521. [CrossRef]
43. Ramsey, E.W., III; Lu, Z.; Rangoonwala, A.; Rykhus, R.P. Multiple Baseline Radar Interferometry Applied to Coastal Land Cover Classification and Change Analyses. *GISci. Remote Sens.* **2006**, *43*, 283–309. [CrossRef]
44. Kim, S.W.; Wdowinski, S.; Amelung, F.; Dixon, T.H.; Won, J.S. Interferometric Coherence Analysis of the Everglades Wetlands, South Florida. *IEEE Trans. Geosci. Remote Sens.* **2013**, *51*, 5210–5224. [CrossRef]